The late ISC pathway interactome reveals mitosomal-cytoplasmic crosstalk in *Giardia intestinalis*

Alžběta Motyčková[1], Luboš Voleman[1], Vladimíra Najdrová[1], Lenka Marková[1], Martin Benda[1], Vít Dohnálek[1], Natalia Janowicz[1], Ronald Malych[1], Róbert Šuťák[1], Thijs J. G. Ettema[2], Staffan Svärd[3], Courtney W. Stairs[4#] and Pavel Doležal[1#]

[1]Department of Parasitology, Faculty of Science, Charles University, BIOCEV, Průmyslová 595, 252 50, Vestec, Czech Republic

[2]Laboratory of Microbiology, Wageningen University and Research, Wageningen, The Netherlands

[3] Department of Cell and Molecular Biology, Biomedical Center (BMC), Uppsala University, Uppsala, Sweden.

[4]Department of Biology, Lund University Lund, Sweden

#Authors for correspondence:

Courtney Stairs: courtney.stairs@biol.lu.se

Pavel Doležal: pavel.dolezal@natur.cuni.cz

ABSTRACT

Mitochondrial metabolism is entirely dependent on the biosynthesis of the [4Fe-4S] clusters, which are part of the subunits of the respiratory chain. The mitochondrial late ISC pathway mediates the formation of these clusters from simpler [2Fe-2S] molecules and transfers them to client proteins. Here, we characterized the late ISC pathway in one of the simplest

mitochondria, mitosomes, of the anaerobic protist *Giardia intestinalis* that lost the respiratory chain and other hallmarks of mitochondria. Identification of the late ISC interactome revealed unexpected involvement of the aerobic marker protein BolA and specific interaction of IscA with the outer mitosomal membrane. Although we confirmed that the synthesis of the Fe-S cluster remained the only metabolic role of mitosomes, we also showed that mitosomes lack client proteins that require the [4Fe-4S] cluster. Instead, by knocking out the *bolA* gene from the *G. intestinalis* genome, we showed that, unlike aerobic mitochondria, the late ISC mitosomal pathway is involved in the assembly of cytosolic [4Fe-4S] clusters. Thus, this work reveals an unexpected link between the formation of mitochondrial and cytosolic [4Fe-4S] clusters. This may either be a consequence of mitochondrial adaptation to life without oxygen, or it represents a general metabolic coupling that has not been previously observed in the complex mitochondrial metabolism of aerobes.

INTRODUCTION

Giardia intestinalis is a microaerophilic parasitic protist that lives in the epithelium of the small intestine of mammals, where it causes giardiasis (1). It belongs to the Metamonada supergroup of eukaryotes that typically contain mitochondria-related organelles (MRO) that lack organellar genomes and cristae and that are adapted to life with little or no oxygen (2). The so-called mitosomes of *G. intestinalis* are one of the simplest MROs known among eukaryotes, as they contain only a single metabolic pathway for iron-sulfur (Fe-S) cluster synthesis (ISC) (3–5).

Fe-S clusters function as cofactors of proteins (Fe-S proteins) in all living organism. In eukaryotes, they participate in essential biological processes in various compartments such as DNA maintenance in the nucleus, electron transport chains in mitochondria, and protein

translation in the cytoplasm (6–8). In humans, about 70 different Fe-S proteins have been identified (7).

In aerobic eukaryotes, the formation of Fe-S clusters for all cellular proteins begins in mitochondria via the activity of the ISC pathway, which can be functionally divided into the early or late acting complex of proteins (9). In 'classical' mitochondria (Fig. 1A), the early ISC pathway produces [2Fe-2S] clusters on the scaffold protein IscU (10) via the activity of a complex consisting of cysteine desulfurase IscS (11), its accessory subunit Isd11 (12–14) and an acyl carrier protein (15–17). The actual transfer of sulfur to IscU is facilitated by frataxin (18) and the electrons for cluster formation are provided by reduced ferredoxin (Fdx), which itself is a [2Fe-2S] protein (19). However, the source of iron and the mechanism of iron transfer to the cluster remain elusive. Upon the formation of [2Fe-2S] cluster on IscU, a chaperone complex consisting of Hsp70 and HscB transfers the cluster to glutaredoxin 5 (Grx5) apoprotein (20).

Grx5 acts as the central dividing point between the early and late ISC pathway at which the assembled [2Fe-2S] cluster is either (i) transferred to the target mitochondrial [2Fe-2S] apoproteins, (ii) exported to the cytosol as an enigmatic X-S compound or (iii) enters the late ISC machinery (9,21). The late ISC machinery starts with the transfer of two [2Fe-2S] clusters from Grx5 to a complex of IscA1, IscA2 and Iba57 (22) where the [4Fe-4S] cluster is formed (23). The newly created [4Fe-4S] clusters are delivered to apoproteins with the help of Nfu1 (24,25) and Ind1, the latter being specifically involved in [4Fe-4S] cluster-binding for the complex I assembly (26). Recently, two conserved factors BolA1 and BolA3 have been shown to participate in the transfer of [4Fe-4S] clusters to apoproteins in mitochondria (27). BolA1 and BolA3 have overlapping functions, but preferentially act on Grx5 and Nfu1,

73 respectively (25). Importantly, BolA function has previously been associated with aerobic
74 metabolism, which was supported by its absence in anaerobic eukaryotes (28).

75 It is now generally accepted that the early ISC pathway is a converging evolutionary
76 point of the MROs, *i.e.*, no matter how much the mitochondrion has been modified during
77 evolution, most MROs have retained early ISC components like IscU and IscS (29).
78 Moreover, some of the MROs like mitosomes of *G. intestinalis* also contain components of
79 the late ISC pathway.

80 Therefore, here, we sought to experimentally examine the nature of the late ISC
81 pathway in *G. intestinalis.* Using enzymatic tagging and series of affinity pulldowns, we have
82 generated a robust interactome of the mitosomal late ISC pathway revealing that Grx5, Nfu1
83 and herein discovered BolA orthologue are at the core of the pathway. On the other hand,
84 mitosomal IscA appears to function in downstream steps of the pathway. The specific
85 interaction between BolA and Grx5 could be confirmed by yeast two hybrid assays as well as
86 by their strict co-occurrence in other MRO-carrying species. However, no endogenous
87 mitosomal substrate for the late ISC pathway could be identified in the mitosomal proteome
88 or in the bioinformatic search of the *G. intestinalis* genome. Hence, a complete *bolA* knockout
89 strain was generated by CRISPR/Cas9 which showed a significantly decreased activity of
90 cytosolic [4Fe-4S] pyruvate:ferredoxin oxidoreductase. These results indicate that mitosomal
91 BolA, and thus the late ISC pathway, is required for the formation of cytosolic [4Fe-4S]
92 clusters. Such functional connection is unknown for mitochondria and may represent unique
93 of adaptation of MROs.

94

95 **RESULTS**

96

97 **The late ISC pathway and the identification of BolA in *G. intestinalis***

Previous genomic and proteomic analyses of *G. intestinalis* revealed the presence of three late ISC pathway components; Nfu1, IscA and Grx5, hereafter referred to as *Gi*Nfu1, *Gi*IscA, and *Gi*Grx5, respectively (Fig. 1A). All three proteins possess highly conserved cysteine residues that are necessary for the coordination of the Fe-S cluster. *Gi*Grx5 contains the CGFS motif of monothiol glutaredoxins (Fig. 1B, Supplementary Fig. 1A), the C-terminal domain of *Gi*Nfu1 carries a CxxC motif (Fig. 1B and Supplementary Fig. 1B) and *Gi*IscA carries a Cx_nCxC signature motif (Fig. 1B, Supplementary Fig. 1C). Both *Gi*Nfu1 and *Gi*IscA carry a short N-terminal pre-sequence that likely serves as the mitosomal targeting signal. *Gi*Grx5 was previously shown to carry a long non-homologous N-terminal sequence, which is required for targeting but may possibly play an additional role in protein function (30). Of the two types of IscA proteins known for eukaryotes, only IscA2 was identified in *G. intestinalis* (4).

The presence of these three late ISC components in *G. intestinalis* prompted us to search for other factors that were identified within the late pathway. Specifically, the orthologues of BolA, Iba57 and Ind1 proteins were searched using hidden Markov model (HMM) profiles against the *G. intestinalis* genome. Interestingly, while the last two searches did not result in the identification of positive hits, a single BolA orthologue was identified in *G. intestinalis* (*Gi*BolA) (Fig. 1B, 1C). The protein could be readily identified in the conceptual proteomes of all genotypes (assemblages) including new genome assembly of WBc6 (31) but was missing from the original reference genome, probably due to its small size (32). The amino acid sequence of *Gi*BolA contains signature V/I/LHAL/I motif towards the C-terminus (33) but no putative N-terminal targeting sequence, as is common to most other BolA proteins (e.g., Fig. 1C). Structural prediction of *Gi*BolA using AlphaFold 2 revealed an αβαβ topology that matches experimentally solved or predicted structures of BolA homologs from both eukaryotes and prokaryotes (Fig. 1D) (34,35). The only structural difference is a

short C- terminal α-helix missing in *Gi*BolA (Fig. 1D). Given the occurrence of three BolA proteins in eukaryotes, phylogenetic analysis was performed to determine which of three eukaryotic BolA paralogues, functioning in the cytosol (BolA2) (36) or mitochondria (BolA1 and BolA3) (28,37) is present in *G. intestinalis.* The analysis showed that *Gi*BolA and other BolA proteins that could be identified in the Metamonada supergroup emerge from within a clade of BolA1 proteins (Fig. 1E) suggesting that *G. intestinalis* contains an orthologue of mitochondrial BolA1, which would hence be expected to be localized in mitosomes.

_Gi_BolA is part of mitosomal late ISC pathway.

To test whether *Gi*BolA is indeed a mitosomal component, the protein was expressed with the C-terminal biotin acceptor peptide tag (BAP) tag. Immunodetection of the tag by fluorescence microscopy showed clear colocalization of *Gi*BolA with the mitosomal marker GL50803_9296 (Fig. 2A). Western blot analysis of the cellular fractions revealed the specific presence of the protein in the high-speed pellet (HSP) fraction that is enriched for mitosomes (Fig. 2B). Except for *Gi*Grx5 (30), the mitosomal localization of other late ISC components had not been previously experimentally confirmed. Therefore, analogously, all three proteins were expressed with the C-terminal BAP tag and their cellular localization was detected in the fixed cells (Fig.2A) and in the cell fractions (Fig. 2B). All proteins specifically localize in the mitosomes. Furthermore, we tested whether BAP-tagged proteins are localized within the mitosomes or are accumulated on the surface of the organelle as a possible result of protein overexpression. To this end, a protease protection assay was performed on *G. intestinalis* expressing BAP-tagged proteins whereby HSPs were incubated with trypsin in presence or absence of a membrane-solubilizing detergent. Proteins encased by one or more membranes will be inaccessible to trypsin and will therefore be detected by standard immunoblotting in the absence but not presence of the detergent (Fig. 2C). Unlike the outer membrane marker

148 *Gi*Tom40, all late ISC components were resistant to protease treatment as the mitosomal
149 matrix marker IscU. As a control, mitosomal membrane solubilization resulted in overall
150 protein degradation. In summary, all four proteins were found specifically located within
151 mitosomes, suggesting that the minimalist late ISC pathway occurs within the organelles.
152
153 **Mitosomal BolA specifically interacts with Grx5 and other mitosomal ISC components.**
154 Recent studies on human BolA proteins showed a specific interaction of mitochondrial
155 BolA1 with Grx5 during the stabilization of [2Fe-2S] cluster on Grx5 (27). Using a yeast two
156 hybrid (Y2H) assay, we tested whether mitosomal BolA also interacts with Grx5. Indeed, the
157 assay was able to show the interaction between *Gi*BolA and *Gi*Grx5 (Fig. 2D). Previous
158 studies in yeast identified the specific residues of BolA and Grx5 critical for interaction (27).
159 Therefore, we tested whether the same molecular interaction can also be demonstrated for the
160 *Giardia* proteins. Specifically, the cysteine residue (position 128) within the CGFS motif of
161 *Gi*Grx5 and a highly conserved histidine residue (position 82) of *Gi*BolA, that were both
162 shown to coordinate Fe-S cluster (38). In both cases, the introduced mutations abolished the
163 positive interaction in Y2H (Fig. 2D). These results strongly suggest that the mechanism of
164 interaction is conserved for the late ISC components in the *G. intestinalis* mitosomes.
165 However, the analogous assay did not show any interaction between *Gi*BolA and *Gi*Nfu1
166 (data not shown), that would be expected if *Gi*BolA represented a BolA3 homologue (25)
167 To reveal the complex *in vivo* interactions of *Gi*BolA, we used a previously
168 established method of enzymatic tagging in *G. intestinalis* that is based on co-expression of
169 the biotin ligase (BirA) and protein of interest tagged by BAP (3). In the presence of ATP,
170 BirA specifically biotinylates the lysine residue within the BAP tag. Therefore, a BAP-tagged
171 *Gi*BolA was introduced into *G. intestinalis* expressing cytosolic BirA. The mitosomes-
172 enriched HSP was incubated with the chemical crosslinker DSP and *Gi*BolA-BAP was

purified on streptavidin-coupled magnetic beads (see Materials and Methods for more details). The purified crosslinked complexes were subjected to proteomic analysis and the resulting peptide mass spectra were searched against the predicted proteome of *G. intestinalis* (39). Data obtained from the biological and technical triplicates (Supplementary Table 1) were displayed in a volcano plot showing the fold change of protein abundance compared to the negative control (Fig. 2E). In total, 26 significantly-enriched proteins were identified. *Gi*Grx5 represented the most enriched interactor but other ISC components (NifU, IscA, Fdx, IscU, IscS, Hsp70, Jac1) also appeared among the most significant enriched proteins (Fig. 2E). The remaining proteins represented mitosomal proteins involved in protein import and folding, and mitosomal proteins of unknown function. At least one probable non-mitosomal protein (PSMC1, Proteasome 26S Subunit, ATPase 1 homologue) was identified among the significantly enriched proteins (Fig. 2E, Supplementary Table 1) suggesting minimal contamination from non-mitosomal proteins in this proximity tagging method. The dominant presence of mitosomal matrix proteins in the presented interactome strongly suggests that *Gi*BolA is localized in the mitosomal matrix. This represents the first report of a BolA protein and putative late ISC pathway in an anaerobic mitochondrial organelle.

Co-occurrence of mitochondrial BolA and Grx5 and a uniform pattern of late ISC components in metamonads

All known eukaryotic organisms belonging to the Metamonada supergroup of eukaryotes carry MROs adapted to life without oxygen. According to genomic and transcriptomic analyses, the degree of metabolic reduction of these MROs varies across the Metamonada (40,41). Some MROs participate in ATP generation and some, such as *G. intestinalis* mitosomes, are involved only in the synthesis of Fe-S clusters. The identification of *Gi*BolA prompted us to search the available data for the homologues of BolA and other ISC components in Metamonada.

A BolA homologue was detected in genomes of the parasitic *Giardia muris* and two *Retortamonas* species, and in free-living *Dysnectes brevis*, *Kipferlia bialata* and *Aduncisulcus paluaster* (Fig. 2F, Supplementary Table 2). Similarly to *G. intestinalis*, the vast majority of Metamonada have been found to lack Iba57 and IscA1. The absence of the former correlates with the absence of complex I in these eukaryotes, but both Iba57 and IscA1 are supposed to constitute a complex together with IscA2, on which the [4Fe-4S] cluster is formed (42) This raises the general question whether IscA2, unlike the whole IscA1-IscA2-Iba57 complex, has an indispensable role for anaerobic eukaryotes. Analogously, we could not detect the early ISC components Isd11 and ferredoxin reductase (Arh1) in preaxostylids and fornicates (Fig. 2F). These components were only detected in the less reduced MROs of parabasalids (e.g., *Trichomonas vaginalis*) and in anaeramoebids. Of course, additional components can be identified in the species with incomplete genomic data, yet these results likely demonstrate the ancestral adaptation of the late ISC pathway in Metamonada that involved the loss of Iba57 and IscA proteins.

Interactome of late ISC components reveals a downstream role of IscA

Characterization of late ISC pathway in mitochondria has relied largely on genetic and biochemical approaches *e.g.*, (25–27,43–45). Here, we chose to continue with the affinity-purification proteomics, which to our knowledge has not yet been used in this context, to characterize the pathway in *G. intestinalis* mitosomes. The combination of protein specific interactomes as the one obtained above for *Gi*BolA can yield a spatial reconstruction of the pathway (46). In addition, it can also identify putative mitosomal client apoprotein(s) that receive the synthesized [4Fe-4S] clusters as it was done for its mitochondrial counterparts (25,47). To this aim, proteins co-purified in complexes chemically crosslinked to *Gi*Grx5, *Gi*Nfu1, and *Gi*IscA were identified by mass spectrometry. The returned datasets contained

47, 30, and 22 statistically significant proteins of three independent sets of experiments, respectively (Fig. 3A-C, Supplementary Table 1).

The final combined dataset which also included the *Gi*BolA purification data was plotted in a heat map using log2 transformed fold difference values (Fig. 3D). Hierarchical clustering showed a close relationship between the *Gi*BolA-, *Gi*Nfu1- and *Gi*Grx5-specific protein profiles, while the *Gi*IscA-specific dataset remained the most distinct. The interactomes of the first three proteins converged over the ISC components, chaperones and the mitosomal processing peptidase (GPP) that corresponds to the 'core' of the mitosomal metabolism (dashed line in Fig 3D). Several low abundance proteins of unknown function (GL50803_21201, GL50803_16424 and ABC transporter GL50803_87446) were also found in the cluster. Interestingly, a thioredoxin reductase (TrxR) homolog (GL50803_9287) was found among several proteins unique to the *Gi*Grx5 dataset (Fig. 3B). The protein was previously characterized in *G. intestinalis* as cytosolic protein, yet without any interacting thioredoxin (48). Our data suggested that TrxR thus could also act in the mitosomes and reduce *Gi*Grx5 to act as a missing reductase system. *Gi*BolA was found among enriched proteins in *Gi*Grx5 and *Gi*Nfu1 datasets (Fig. 3A, 3B) yet it was not a significant hit due to the incomplete coverage in some of the technical triplicates within biological triplicates. This indicates lower expression levels of *Gi*BolA when compared to other late ISC components.

In contrast, the *Gi*IscA dataset showed enrichment of the outer mitosomal membrane proteins MOMP35 and GL50803_17276 (3,49). Additionally, Tom40, a central component of the outer membrane translocase, was identified among the significantly enriched proteins (Supplementary table 1). Unlike the interactomes of the other ISC components, many of the 'core' mitosomal matrix proteins were not significantly enriched in the GiIscA interactome. The affinity of *Gi*IscA to the outer membrane proteins suggested the possibility that the protein is not localized, at least not completely, in the mitosomal matrix but in the

intermembrane space (IMS) or it is associated with the outer mitosomal membrane. The latter could be rejected due to the lack of any transmembrane domains and due to the full protection of *Gi*IscA against the externally added protease (Fig. 2C). Therefore, the presence of the protein in the IMS was tested. We took advantage of differential sensitivity of the outer and inner mitosomal membranes to digitonin lysis (3,50).

The mitosome-enriched fraction was isolated from cells co-expressing *Gi*IscA and the matrix marker *Gi*IscU and incubated with the increasing concentration of digitonin. The release of the proteins from the organelles was monitored via Western blot (Fig. 3E). Interestingly, *Gi*IscA showed a greater proportion of protein released into the supernatant fraction than *Gi*IscU, supporting the hypothesis that *Gi*IscA and *Gi*IscU are not in the same mitosomal subcompartment.

Mitosomes likely lack the [4Fe-4S] client for the late ISC pathway

The late-acting ISC machinery is responsible for the formation of [4Fe-4S] cluster and its delivery to the client apoproteins within the mitochondrion of model eukaryotes. These include many mitochondrial proteins functioning in the electron transport chain, the TCA cycle, and cofactor biosynthesis (51–54). However, all these proteins are absent in the highly reduced *G. intestinalis* mitosomes.

To identify possible mitosomal clients of the late ISC pathway, we first investigated the interactome of *Gi*Nfu1 with the premise that the apoproteins that receive their [4Fe-4S] cluster from the late ISC pathway can be co-purified with Nfu1 (25,47,55). The search in the dataset for [4Fe-4S] cluster motifs (56) did not return any positive hits, therefore an unbiased search for Fe-S proteins within the entire conceptual *G. intestinalis* cellular proteome was performed by MetalPredator (57). Upon manual checking with available literature and structural information, 40 proteins were identified that bind [4Fe-4S] clusters (Fig. 4A, Supplementary Table 3). Of these, 19 were predicted to function in the cytosol in energy,

redox, amino acid, and nitrogen metabolism, as well as cofactor biosynthesis and protein translation. There were 11 nuclear proteins identified, participating either in DNA or RNA metabolism. The remaining components corresponded to the transient cluster carriers of the mitosomal ISC machinery and cytosolic iron–sulfur assembly (CIA) pathway (58). The only mitosomal protein with stably associated Fe-S cluster is [2Fe-2S] ferredoxin, which is itself directly involved in the ISC pathway as an electron carrier. Of course, we cannot rule out the presence of a previously unknown protein with a unique cluster binding domain/motif in mitosomes, but the present data suggest that mitosomes lack any client [4Fe-4S] protein for their late ISC pathway.

Knockout of *bolA* gene is manifested by a decrease in the activity of the cytosolic [4Fe-4S] containing PFOR.

BolA was previously thought to be restricted to aerobic eukaryotes (28), thereby all functional analyses have been performed on aerobic model organisms (59). Having established the integration of *Gi*BolA within the mitosomal late ISC pathway, we next examined the role of BolA in the formation of Fe-S clusters. To this aim, using the recently established CRISPR/Cas9-mediated gene knockout approach (60) and a *G. intestinalis* cell line lacking *bolA* gene (ΔbolA) was generated (Fig. 4B, 4C). The gene knockout was verified by PCR on the gDNA for the absence of *bolA* gene and the presence of homologous recombination cassette (HRC) (Fig. 4B). Furthermore, no *bolA* mRNA was detected in cDNA prepared from the cells (Fig. 4C). Finally, the proteomic analysis of mitosomes-enriched HSP fraction showed the absence of BolA when compared to the control (Supplementary Table 4).

The ΔbolA cell line exhibited slowed growth when compared to the parental cells (Cas9) and the wild-type control (WBc6) (Fig. 4D) but the overall number and morphology of the

mitosomes remained unchanged (Fig. 4E, Supplementary Fig. 2). This indicated that disruption of the function of late ISC pathway can perturb growth rate but not mitosomal morphology or number in *G. intestinalis*. Given the apparent absence of the client proteins in the mitosomes, the formation of [4Fe-4S] clusters was monitored indirectly via the activity of cytosolic enzyme pyruvate-ferredoxin oxidoreductase (PFOR). PFOR catalyses oxidative decarboxylation of pyruvate and produces acetyl-CoA and CO_2 with concomitant reduction of cytosolic ferredoxin (another [4Fe-4S]-containing protein), hence acting as cytosolic alternative of pyruvate dehydrogenase complex in mitochondria of aerobes (61). Indeed, the specific activity of PFOR was more than three times lower in ΔbolA cells when compared to the control (Fig. 4F). The expression of two *pfor* genes present in *G. intestinalis* genome was measured by qPCR and found almost unchanged in the ΔbolA cells (Fig. 4G). Taken together, these data strongly suggested that the absence of mitosomal BolA impacts the formation of [4Fe-4S] clusters in *G. intestinalis* cytosol.

DISCUSSION

This study presents the characterization of late ISC pathway in anaerobic protist *G. intestinalis*. While it shows an unexpected presence of BolA in its mitosomes, it also demonstrates the involvement of the mitosomes in the formation of Fe-S clusters for cytosolic proteins. Thus, this is the first study supporting the long-proposed hypothesis of MROs as evolutionarily conserved compartments dedicated to control Fe-S cluster biogenesis. Moreover, it shows that, unlike in mitochondria, the defect in the late ISC pathway of *G. intestinalis* mitosomes affects the activity of Fe-S proteins outside the organelle.

The independent evolution of mitochondria in various anaerobic lineages of eukaryotes resulted into remarkably uniform metabolic adaptations. Comparative studies on mitochondria and various MROs have suggested that the mitochondrial formation of Fe-S

clusters was the main selection pressure for retaining the organelles even in the anoxic environments (5,62–66). Mitochondria initiate the biosynthesis of cellular Fe-S clusters via the action of early ISC components that results into the formation of [2Fe-2S] cluster bound by glutaredoxin (Grx5) dimer. From here, the cluster is either distributed to mitochondrial clients, combined via late ISC components to [4Fe-4S] clusters or exported as an unknown sulfur-containing factor to the cytosol (63). Most of mitochondrial Fe-S client proteins contain [4Fe-4S] clusters and thus the late ISC pathway is vital for the function of the respiratory chain, the TCA cycle as well as the synthesis of prosthetic groups such as heme, lipoic acid or molybdenum cofactor (63). Number of late ISC components are dedicated to serve these multiple clients in mitochondria and some of them could be also identified in *G. intestinalis.*

In this study, we show that despite the loss of all mitochondrial pathways that require the presence of [4Fe-4S] clusters, mitosomes of *G. intestinalis* contain four late ISC components; Grx5, IscA, Nfu1 and the newly identified BolA homologue. In classical experimental models of yeast and mammalian mitochondria, defective late ISC pathway is often lethal for the cell or at least lead to severe diseases in humans due to multifactorial deficiencies caused in the mitochondrial metabolism (67,68). In this context, mitosomes represent a unique biological model to study the non-mitochondrial role of the ISC pathway without the interference with mitochondrial metabolism.

Eukaryotes have three BolA proteins that function together with glutaredoxins in chaperoning the Fe-S cluster both in cytosol and mitochondria (25,27,69). Yet, the previous absence of BolA proteins in the anaerobic eukaryotes that carry MROs suggested that BolA proteins are involved in the aerobic metabolism by controlling thiol redox potential (28). Mitochondrial BolA1 and BolA3 were proposed to function as [4Fe-4S] assembly cluster factors via the interaction with Grx5 and Nfu1, respectively (25,27,70). While the BolA3-

Nfu1 interaction is required for the final [4Fe-4S] cluster transfer to the apoprotein (Melber et al. 2016), the exact role of BolA1-Grx5 in the preceding steps remains rather unknown. *Gi*BolA specifically interacts with *Gi*Grx5 as demonstrated by Y2H assay and the pulldown experiment. The interaction of *Gi*BolA with *Gi*Nfu1 was not supported by Y2H assay, yet the *Gi*Nfu1 was among the most enriched proteins co-purified with *Gi*BolA. These data indirectly support the results of the phylogenetic reconstructions assigning *Gi*BolA to BolA1 proteins. Interestingly, the search in other anaerobic organisms with MROs revealed co- occurrence of BolA and Grx5 homologues, supporting their mutual interaction in the pathway. However, for yet unknown reason the pair is expendable in some Metamonada species, some of which carry metabolically versatile ATP-producing MROs, *e.g.,* the parabasalids and anaeramoebids.

Based on this data and the existence of BolA deficient yeast cell lines that exhibited relatively mild phenotype (27), the gene was selected for the targeted removal from *G. intestinalis* genome by CRISPR/Cas9. The assumption was that the gene would not be essential for *G. intestinalis* either. In addition, such a viable mutant could also reveal a general function of mitosomes in Fe-S cluster formation. Indeed, removal of the gene encoding *Gi*BolA by CRISPR/Cas9 showed that this protein is not essential for *G. intestinalis* maintained under laboratory conditions. The ΔbolA cell line showed a growth defect that was not associated with reduced mitosomal biogenesis, consistent with the previous observation that *G. intestinalis* does not respond to metabolic perturbations by altering mitosomal dynamics (71). In yeast and patient-derived cell lines, BolA deficiency is manifested by a decrease in the activity of the [4Fe-4S] cluster containing protein succinate dehydrogenase, but also of pyruvate and 2-ketoglutarate dehydrogenases due to impaired lipoylation by [4Fe-4S] lipoate synthase (27,37). Since *Giardia* does not encode any of these proteins or any other obvious mitosomal [4Fe-4S] protein, we explored whether BolA deficiency could be manifested in the activity of cytosolic [4Fe-4S] proteins. We found that the cytosolic [4Fe-4S]

PFOR had significantly reduced enzymatic activity in cells lacking BolA compared to the control cell line. Transcription of the two *pfor* genes was nearly identical in the ΔbolA cell line, strongly suggesting that the lack of mature [4Fe-4S] cluster in the protein is responsible for the reduced enzymatic activity. These data demonstrate, for the first time, that mitosomes are needed for cytosolic Fe-S cluster biogenesis in *G. intestinalis.* As *Gi*BolA is the first ISC component removed from *G. intestinalis,* it is difficult to assess whether the reduced PFOR activity is a direct consequence of *Gi*BolA deficiency or a broader downstream outcome of a defect in Fe-S cluster formation.

In model aerobic eukaryotes, there is an additional cytosolic acting BolA protein (BolA2) and glutaredoxin (Grx??? Is this known?) that act as chaperones for cytosolic Fe-S clusters. It is thus possible that the single BolA protein of *G. intestinalis* also effects cytosolic Fe-S clusters. However, further studies are needed to understand the actual connection between the mitosomal late ISC pathway and Fe-S proteins in other cellular compartments. However, it is tempting to speculate that similar connection may exist in the aerobes but has remained unrecognized due the crucial role of the ISC pathway for the mitochondria themselves.

In mitochondria, the Atm1 transporter in the inner membrane was shown to link the early ISC pathway with the cytosolic iron–sulphur assembly (CIA) via the transport of an unknown sulphur-containing molecule (72). Atm1 homologue is missing in *G. intestinalis* and so are any other metabolic transporters or carriers. Thus, surprisingly, *Gi*IscA might have a compensatory role as a candidate for the connection between the cytosolic CIA (58) and mitosomal ISC machinery. The specific interaction of *Gi*IscA with the proteins in the outer mitosomal membrane and the sensitivity to the outer membrane solubilization indicated that it may in fact reside, at least partially, in the IMS of the mitosomes. Although such localization would represent a unique adaptation of *G. intestinalis* mitosomes, it would also correspond to

the loss of client proteins in these organelles. Of course, further experiments are needed to describe the place of action of *Gi*IscA but the obvious complication is the size of the mitosomes and the lack of any IMS markers.

To conclude, this work shows how late ISC pathway has undergone specific functional adaptations in a eukaryote inhabiting anoxic environments. It shows for the first time that the formation of Fe-S clusters within these highly reduced mitochondria has remained functionally important for the cytosolic Fe-S proteins as known for the 'classical' aerobic mitochondria.

MATERIALS AND METHODS

Bioinformatics

The structural models of human and *G. intestinalis* BolA were computed using the Google Colab interface of AlphaFold2 (https://colab.research.google.com/github/sokrypton/ColabFold/blob/main/beta/AlphaFold2_advanced.ipynb) (73). The multiple sequence alignment was generated with the jackhmmer option. The best scoring structure according to the plDDT score was subsequently refined with the Amber-Relax option. The [Fe-S] proteins were predicted by Metalpredator (74) using the conceptual proteome of *G. intestinalis* WBc6 strain (giardiadb.org).

Phylogenetic dataset construction and inferences

Human BolA proteins (NP_001307954.1, NP_001307536.2, NP_997717.2) and Giardia intestinailis BolA-like protein were used as a query against NCBI non-redundant (nr) database to retrieve sequences from select Opishthokonta (Danio renio, Mus musculus, Caenorhabditis elegans Schizosaccharomyces pombe Saccharomyces cerevisiae), select Viridiplantae (Glycine_max Arabidopsis_thaliana Chlamydomonas_reinhardtii Chlorella_variabilis) and

423 non-opisthokonts and non-Viridiplantae (by restricting the database to non-opisthokonts and
424 non-Viridiplantae) with an e-value threshold of $1e^{-3}$. We also examined the predicted
425 proteomes of metamonads available on EukProt
426 (https://www.biorxiv.org/content/10.1101/2020.06.30.180687v2.abstract) and various
427 sequencing intiatives (40,75,76). The resulting queries were clustered based on sequence
428 identity whereby using cd-hit (77) with a cut-off value of 0.9. Sequences were aligned using
429 mafft (--auto) (78) and ambiguously aligned positions were removed using trimal with '-gt
430 0.5'(79). Phylogenetic inference was performed using IQTREE2 to generate 1000 ultrafast
431 bootstraps (-bb 1000) (80) under the LG+C60+G model of evolution (computed using -mset
432 LG+C20,LG+C10,LG+C60,LG+C30,LG+C40,LG+C50,LG). Trees were visualized using
433 FigTree v1.4 and stylized in Adobe Illustrator. Alignments and tree files are available at
434 figshare (https://figshare.com/s/8fbd1368814dbd11192c reserved
435 DOI:10.6084/m9.figshare.19772155).
436
437 **Cloning and protein expression**
438 For the expression of BAP-tagged proteins in *G. intestinalis*, the genes were amplified from
439 genomic DNA and inserted into to pONDRA plasmid encoding the C-terminal BAP tag (81).
440 All the primers and the restriction enzymes used in this study are listed in Supplementary
441 Table 5. Transfection was done as previously described (82) For the *in vivo* biotinylation, the
442 cells expressing BAP-tagged proteins were transfected with a pTG plasmid encoding
443 cytosolic BirA gene from *E. coli* (3). For Y2H assay, genes were amplified from gDNA and
444 subcloned to both pGADT7 and pGBKT7 plasmids. Mutated versions of genes for Y2H assay
445 were commercially synthesized (Genscript).
446 For CRISPR/Cas9-mediated knockout of *bolA* gene, gRNA sequence
447 ATCAGCTCTCCCGACTTCAA was inserted into gRNA cassette of pTGuide vector using

448 (60) two annealed oligonucleotides (see Supplementary Table 5 for primers and restriction
449 enzymes used). The 999 bp of 5´ and 940 bp 3´ homologous arms surrounding *bolA* gene
450 were inserted into pTGuide vector as the homologous arms for the recombination of the
451 resistance cassette (Supplementary Table 5).
452
453 **Real-time PCR**
454 Total RNA from ΔbolA and control cell line was isolated independently six times using
455 NucleoSpinTM RNA isolation kit (Macherey-Nagel) according to manufacturer's protocol.
456 cDNA prepared from these RNA isolations by KAPA SYBR® FAST One-Step kit (Roche)
457 was analyzed directly by qPCR in Real-time PCR cycler RotorGene 3000 (Qiagen) using
458 Rotor-Gene 6.0 software. qPCRs for each gene were performed in technical triplicates in each
459 RNA isolation for both strains and the mean for each gene from individual RNA isolations
460 was used for further calculations. NADH oxidase-encoding gene, GL50803_33769, was used
461 as a housekeeping gene for normalization.
462
463 **Cell culture, fractionation and immunoblot analysis.**
464 Trophozoites of *G. intestinalis* strain WB (ATCC 30957) were grown in TYI-S-33 medium
465 (83) supplemented with 10% heat-inactivated bovine serum (PAA laboratories), 0,1% bovine
466 bile and antibiotics. Cells were harvested and fractionated as previously described (3). Cells
467 expressing BAP-tagged *Gi*BolA, *Gi*Grx5, *Gi*Nfu1, and *Gi*IscA were harvested and
468 fractionated as previously described (3) Briefly, the cells were harvested in ice cold phosphate
469 buffered saline (PBS, pH 7.4) by centrifugation at 1,000 × g, 4 °C for 10 min, washed in SM
470 buffer (20 mM MOPS, 250 mM sucrose, pH 7.4), and collected by centrifugation. Cell pellets
471 were resuspended in SM buffer supplemented with protease inhibitors (Roche). Cells were
472 lysed on ice by sonication for 2 min (1 s pulses, 40 % amplitude). The lysate was centrifuged

at 2,680 × g, for 20 min at 4 °C to sediment the nuclei, cytoskeleton, and remaining unbroken cells. The supernatant was centrifuged at 180,000 × g, for 30 min at 4 °C. The resulting supernatant corresponded to the cytosolic fraction, and the high-speed pellet (HSP) contained organelles including the mitosomes and the endoplasmic reticulum. The *Gi*Nfu1, *Gi*IscA, *Gi*Grx5 and *Gi*BolA proteins were detected by a rabbit anti-BAP polyclonal antibody (GenScript). Mitosomal *Gi*Tom40 and *Gi*IscU were detected with a specific polyclonal antibody raised in rabbits (84). The primary antibodies were recognized by secondary antibodies conjugated with horseradish peroxidase. The signals were visualized by chemiluminescence using an Amersham Imager 600.

Immunofluorescence microscopy

G. intestinalis trophozoites were fixed and immunolabeled as previously described (71,85). The C-terminal BAP tag of localized mitosomal proteins was detected by a rabbit anti-BAP polyclonal antibody (GenScript). Mitosomal marker GL50803_9296 was detected by a rabbit anti- GL50803_9296 polyclonal antibody (3). The primary antibodies were detected by secondary antibodies included: Alexa Fluor 594 donkey anti-rabbit IgG (Invitrogen), Alexa Fluor 488 donkey anti-mouse IgG (Invitrogen). Slides were mounted in Vectashield containing DAPI (Vector Laboratories).

Static images were acquired on Leica SP8 FLIM inverted confocal microscope equipped with 405 nm and white light (470-670 nm) lasers and FOV SP8 scanner using HC PL APO CS2 63x/1.4 NA oil-immersion objective. Laser wavelengths and intensities were controlled by a combination of AOTF (Acousto-Optical Tunable Filter) and AOBS (Acousto-Optical Beam Splitter) separately for each channel. Emitting fluorescence was captured by internal spectrally-tunable HyD detectors. Imaging was controlled by the Leica LAS-X software. Images were deconvolved using SVI Huygens software with the CMLE algorithm.

Maximum intensity projections and brightness/contrast corrections were performed in FIJI ImageJ software (86).

Cross-linking, protein isolation, mass spectrometry (MS)

The HSP (10 mg) isolated from each cell line was collected by centrifugation (30 000 x g, 4°C, 10 min) and resuspend in 1 x PBS supplemented with protease inhibitors (Roche) to protein concentration 1.5 mg/ml. The cross-linker DSP (dithiobis(succinimidyl propionate), ThermoScientific) was added to final 100 µM concentration. The sample was incubated 1 h on ice. Crosslinking was stopped by the addition of 50 mM Tris (pH 8.0) followed by 15 min incubation at RT. The sample was collected by centrifugation (30 000 x g, 10 min, RT) and then resuspended in boiling buffer (50 mM Tris, 1mM EDTA, 1% SDS, pH 7.4) supplemented with protease inhibitors. The sample was then incubated at 80 °C for 10 min, collected by centrifugation and the supernatant was diluted 1/10 in the incubation buffer (50 mM Tris, 150 mM NaCl, 5 mM EDTA, 1% Triton X-100, pH 7.4) supplemented with protease inhibitors. Streptavidin-coupled magnetic beads (50 µL of Dynabeads MyOne Streptavidin C1, Invitrogen) were washed three times in 1 ml of the incubation buffer for 5 min and added to the sample, mixed and incubated for 1 h at room temperature and then incubated overnight with gentle rotation at 4°C. The beads with bound protein were washed three times in the incubation buffer (5 ml) supplemented with 0.1% SDS for 5 min, washed in boiling buffer for 5 min and then washed in the washing buffer (60 mM Tris, 2% SDS, 10% glycerol, 0.1% SDC) for 5 min. Finally, the sample was washed twice in 100 mM TEAB (Triethylammonium bicarbonate, Thermofisher) with 0,1% SDC for 5 min. One tenth of the sample was mixed with SDS-PAGE sample buffer supplemented with 20 mM biotin and incubated in 95°C for 5 min. Experimental controls were tested by immunoblotting and then the sample (dry frozen beads with proteins) was analyzed by mass spectrometry. Control

sample was processed in the same way. Each sample was done in triplicate. Beads with bound proteins were submitted to tandem mass spectrometry (MS/MS) analysis as previously described except without the detergent washing steps (82). In brief, captured samples were released from beads by trypsin cleavage. Peptides were separated by reverse phase liquid chromatography and eluted peptides were converted to gas-phase ions by electrospray and analyzed using an Orbitrap (Thermo Scientific, Waltham, MA) followed by Tandem MS to fragment the peptides through a quadropole for final mass detection. Data was analyzed using MaxQuant (version 1.6.3.4) (87) with a false discovery rate (FDR) of 1% for both proteins and peptides and a minimum peptide length of seven amino acids. The Andromeda search engine (88) was used for the MS/MS spectra search against the latest version of the *G. intestinalis* database from EuPathDb (http:// eupathdb.org/eupathdb/) and a common contaminant database. Modifications were set as follows: Cystein (unimod nr: 39) as static, and methionoine oxidation (unimod: 1384) and protein N terminus acetylation (unimod: 1) as variable. Data analyses were performed using Perseus 1.6.1.3 (89) and visualized as a volcano plot using the online tool VolcaNoseR (fold change 1,significance threshold 2) (90) and as a heatmap using the online tool ClustVis (91).

Protease protection and digitonin solubilization assays

For protease protection assay, cells expressing BAP-tagged *Gi*BolA, *Gi*Grx5, *Gi*Nfu1, and *Gi*IscA were harvested and fractionated as described above. The HSP fraction (150 µg) was resuspended in 20 µl of SM buffer and supplemented with protease inhibitors, or 20 µg/ml of trypsin or 20 µg/ml of trypsin and 0.1% Triton X-100. The samples were incubated 30 min at 25 °C and then processed for SDS-PAGE.

For digitonin solubilization assay, 100 µg of HSP fractions isolated from cells co-expressing HA-tagged *Gi*IscU and BAP-tagged *Gi*IscA were incubated for 30 min on ice with

548 0.01 %, 0.05 %, 0.1 %, digitonin, and without digitonin as a control. The samples were
549 diluted by PBS to 800 µl total volume and collected by centrifugation (30 mins, 180,000 × g,
550 at 4 ° C). The resulting pellets were processed for SDS-PAGE and the supernatants were
551 precipitated by 15 % TCA for 30 min on ice and collected by centrifugation for 30 min at
552 180,000 × g and 4 ° C, the pellets were washed once with 500 µl of ice-cold acetone,
553 centrifuged as before. The samples were resolved by SDS-PAGE, transferred to nitrocellulose
554 membrane and the protein tags were detected by rabbit anti-BAP antibody (Genscript) and rat
555 anti-HA antibody (Roche). The release to mitosomal proteins was quantified by ImageJ (86).

556
557 **Y2H assay**

558 The yeast two-hybrid assay (Y2H) was performed as previously described (92). *S.*
559 *cerevisiae* cells (strain AH109) were co-transformed with two plasmids (pGADT7, pGBKT7)
560 with the following combinations of genes: *Gi*BolA + *Gi*Grx5, *Gi*BolA + *Gi*mGrx5 (C128A-
561 mutated Grx5), *Gi*Grx5 + *Gi*mBolA (H90A-mutated *Gi*BolA). The empty plasmids were used
562 as negative controls. Co-transformants were selected on double dropout plates SD -Leu/-Trp
563 and triple dropout plates SD -Leu/-Trp/-His. The colonies were grown for four days at 30°C.
564 The positive colonies from triple dropout medium were grown overnight at 30 °C, 200 RPM
565 and then the serial dilution test was performed on double and triple dropout plates.

566

567 **ACKNOWLEDGEMENTS**

568 The project was supported by grant from the Czech Science Foundation 20-25417S and
569 project ‘Centre for research of pathogenicity and virulence of parasites’ (No.
570 CZ.02.1.01/0.0/0.0/16_019/0000759) to PD funded by European Regional Development Fund
571 and by a grant from Charles University Grant Agency (project number 1396217) to AM. We
572 acknowledge Imaging Methods Core Facility at BIOCEV, institution supported by the MEYS
573 CR (Large RI Project LM2018129 Czech-BioImaging) and ERDF (project No.

574 CZ.02.1.01/0.0/0.0/18_046/0016045) for their support with obtaining imaging data presented
575 in this paper. CWS was supported in part by European Molecular Biology Organization long-
576 term fellowship (ALTF-997-2015) and the Swedish Research Council (Vetenskapsrådet
577 starting grant 2020-05071).

578

579 **REFERENCES**

580

581 1 Adam RD. Biology of *Giardia lamblia*. Clinical Microbiology Reviews 2001;14:447–
582 75.
583 2 Leger MM, Kolísko M, Stairs CW, Simpson AGB. Mitochondrion-related organelles in
584 free-living protists. In: Tachezy J, editor. Hydrogenosomes and Mitosomes:
585 Mitochondria of Anaerobic Eukaryotes. Microbiology Monographs, 2019, p. 287–308.
586 3 Martincová E, Voleman L, Pyrih J, Žárský V, Vondráčková P, Kolísko M, et al. Probing
587 the biology of *Giardia intestinalis* mitosomes using in vivo enzymatic tagging.
588 Molecular and Cellular Biology 2015;35:2864–74.
589 4 Jedelský P, Doležal P, Rada P, Pyrih J, Smíd O, Hrdý I, et al. The minimal proteome in
590 the reduced mitochondrion of the parasitic protist *Giardia intestinalis*. PLoS One
591 2011;6:e17285.
592 5 Tovar J, León-Avila G, Sánchez LB, Sutak R, Tachezy J, van der Giezen M, et al.
593 Mitochondrial remnant organelles of *Giardia* function in iron-sulphur protein
594 maturation. Nature 2003;426:172–6.
595 6 Fuss JO, Tsai C-L, Ishida JP, Tainer JA. Emerging critical roles of Fe-S clusters in
596 DNA replication and repair. Biochim Biophys Acta 2015;176:139–48.
597 7 Andreini C, Banci L, Rosato A. Exploiting bacterial operons to illuminate human iron-
598 sulfur proteins. Journal of Proteome Research 2016;15:1308–22.

599 8 Fontecave M. Iron-sulfur clusters : ever-expanding roles. Nature Chemical Biology
600 2006;2:171–4.
601 9 Braymer JJ, Lill R. Iron–sulfur cluster biogenesis and trafficking in mitochondria.
602 Journal of Biological Chemistry 2017;292:12754–63.
603 10 Mühlenhoff U, Gerber J, Richhardt N, Lill R. Components involved in assembly and
604 dislocation of iron-sulfur clusters on the scaffold protein Isu1p. The EMBO Journal
605 2003;22:4815–25.
606 11 Shi R, Proteau A, Villarroya M, Moukadiri I, Zhang L, Trempe JF, et al. Structural
607 basis for Fe-S cluster assembly and tRNA thiolation mediated by IscS protein-protein
608 interactions. PLoS Biology 2010;8.
609 12 Adam AC, Bornhövd C, Prokisch H, Neupert W, Hell K. The Nfs1 interacting protein
610 Isd11 has an essential role in Fe/S cluster biogenesis in mitochondria. EMBO Journal
611 2006;25:174–83.
612 13 Wiedemann N, Urzica E, Guiard B, Müller H, Lohaus C, Meyer HE, et al. Essential role
613 of Isd11 in mitochondrial iron-sulfur cluster synthesis on Isu scaffold proteins. EMBO
614 Journal 2006;25:184–95.
615 14 Pandey A, Golla R, Yoon H, Dancis A, Pain D. Persulfide formation on mitochondrial
616 cysteine desulfurase: Enzyme activation by a eukaryote-specific interacting protein and
617 Fe-S cluster synthesis. Biochemical Journal 2012;448:171–87.
618 15 Cory SA, Van Vranken JG, Brignole EJ, Patra S, Winge DR, Drennan CL, et al.
619 Structure of human Fe-S assembly subcomplex reveals unexpected cysteine desulfurase
620 architecture and acyl-ACP-ISD11 interactions. Proc Natl Acad Sci U S A
621 2017;114:E5325–34.

16 Van Vranken JG, Jeong MY, Wei P, Chen YC, Gygi SP, Winge DR, et al. The mitochondrial acyl carrier protein (ACP) coordinates mitochondrial fatty acid synthesis with iron sulfur cluster biogenesis. Elife 2016;5.

17 Maio N, Jain A, Rouault TA. Mammalian iron–sulfur cluster biogenesis: Recent insights into the roles of frataxin, acyl carrier protein and ATPase-mediated transfer to recipient proteins. Current Opinion in Chemical Biology 2020;55:34–44.

18 Bridwell-Rabb J, Fox NG, Tsai CL, Winn AM, Barondeau DP. Human frataxin activates Fe-S cluster biosynthesis by facilitating sulfur transfer chemistry. Biochemistry 2014;53:4904–13.

19 Webert H, Freibert SA, Gallo A, Heidenreich T, Linne U, Amlacher S, et al. Functional reconstitution of mitochondrial Fe/S cluster synthesis on Isu1 reveals the involvement of ferredoxin. Nature Communications 2014;5.

20 Maio N, Rouault TA. Mammalian Fe-S proteins: Definition of a consensus motif recognized by the co-chaperone HSC20. Metallomics 2016;8:1032–46.

21 Mühlenhoff U, Braymer JJ, Christ S, Rietzschel N, Uzarska MA, Weiler BD, et al. Glutaredoxins and iron-sulfur protein biogenesis at the interface of redox biology and iron metabolism. Biological Chemistry 2020;401:1407–28.

22 Gelling C, Dawes IW, Richhardt N, Lill R, Muhlenhoff U. Mitochondrial Iba57p is required for Fe/S Cluster formation on aconitase and activation of radical SAM enzymes. Molecular and Cellular Biology 2008;28:1851–61.

23 Brancaccio D, Gallo A, Mikolajczyk M, Zovo K, Palumaa P, Novellino E, et al. Formation of [4Fe-4S] clusters in the mitochondrial iron-sulfur cluster assembly machinery. J Am Chem Soc 2014;136:16240–50.

24 Cai K, Liu G, Frederick RO, Xiao R, Montelione GT, Markley JL. Structural/functional properties of human NFU1, an intermediate [4Fe-4S] carrier in human mitochondrial iron-sulfur cluster biogenesis. Structure 2016;24:2080–91.

25 Melber A, Na U, Vashisht A, Weiler BD, Lill R, Wohlschlegel JA, et al. Role of Nfu1 and Bol3 in iron-sulfur cluster transfer to mitochondrial clients. Elife 2016;5.

26 Bych K, Kerscher S, Netz DJA, Pierik AJ, Zwicker K, Huynen MA, et al. The iron-sulphur protein Ind1 is required for effective complex I assembly. EMBO Journal 2008;27:1736–46.

27 Uzarska MA, Nasta V, Weiler BD, Spantgar F, Ciofi-Baffoni S, Saviello MR, et al. Mitochondrial Bol1 and Bol3 function as assembly factors for specific iron-sulfur proteins. Elife 2016;5.

28 Willems P, Wanschers BFJ, Esseling J, Szklarczyk R, Kudla U, Duarte I, et al. BOLA1 Is an aerobic protein that prevents mitochondrial morphology changes induced by glutathione depletion. Antioxidants & Redox Signaling 2013;18:129–38.

29 Roger AJ, Muñoz-Gómez SA, Kamikawa R. The origin and diversification of mitochondria. Current Biology 2017;27:R1177–92.

30 Rada P, Šmíd O, Sutak R, Doležal P, Pyrih J, Žárský V, et al. The monothiol single-domain glutaredoxin is conserved in the highly reduced mitochondria of *Giardia intestinalis*. Eukaryotic Cell 2009;8:1584–91.

31 Xu F, Jex A, Svärd SG. A chromosome-scale reference genome for *Giardia intestinalis* WB. Scientific Data 2020;7:38.

32 Morrison HG, McArthur AG, Gillin FD, Aley SB, Adam RD, Olsen GJ, et al. Genomic minimalism in the early diverging intestinal parasite *Giardia lamblia*. Science 2007;317:1921–6.

669 33 Li H, Outten CE. Monothiol CGFS glutaredoxins and BolA-like proteins: [2Fe-2S]
670 binding partners in iron homeostasis. Biochemistry 2012;51:4377–89.
671 34 Kasai T, Inoue M, Koshiba S, Yabuki T, Aoki M, Nunokawa E, et al. Solution structure
672 of a BolA-like protein from *Mus musculus*. Protein Sci 2004;13:545–8.
673 35 Chin KH, Lin FY, Hu YC, Sze KH, Lyu PC, Chou SH. NMR structure note – Solution
674 structure of a bacterial BolA-like protein XC975 from a plant pathogen *Xanthomonas*
675 *campestris* pv. *campestris*. Journal of Biomolecular NMR 2005 31:2 2005;31:167–72.
676 36 Kumánovics A, Chen OS, Li L, Bagley D, Adkins EM, Lin H, et al. Identification of
677 FRA1 and FRA2 as genes involved in regulating the yeast iron regulon in response to
678 decreased mitochondrial iron-sulfur cluster synthesis. Journal of Biological Chemistry
679 2008;283:10276–86.
680 37 Cameron JM, Janer A, Levandovskiy V, MacKay N, Rouault TA, Tong WH, et al.
681 Mutations in iron-sulfur cluster scaffold genes NFU1 and BOLA3 cause a fatal
682 deficiency of multiple respiratory chain and 2-oxoacid dehydrogenase enzymes.
683 American Journal of Human Genetics 2011;89:486–95.
684 38 Li H, Mapolelo DT, Randeniya S, Johnson MK, Outten CE. Human glutaredoxin 3
685 forms [2Fe-2S]-bridged complexes with human BolA2. Biochemistry 2012;51:1687–
686 96.
687 39 Aurrecoechea C, Barreto A, Basenko EY, Brestelli J, Brunk BP, Cade S, et al.
688 EuPathDB: the eukaryotic pathogen genomics database resource. Nucleic Acids
689 Research 2017;45:D581–91.
690 40 Leger MM, Kolisko M, Kamikawa R, Stairs CW, Kume K, Čepička I, et al. Organelles
691 that illuminate the origins of *Trichomonas* hydrogenosomes and *Giardia* mitosomes.
692 Nat Ecol Evol 2017;1:0092.

693 41 Stairs CW, Táborský P, Salomaki ED, Kolisko M, Pánek T, Eme L, et al.
694 Anaeramoebae are a divergent lineage of eukaryotes that shed light on the transition
695 from anaerobic mitochondria to hydrogenosomes. Current Biology 2021;31:5605-
696 5612.e5.
697 42 Weiler BD, Brück MC, Kothe I, Bill E, Lill R, Mühlenhoff U. Mitochondrial [4Fe-4S]
698 protein assembly involves reductive [2Fe-2S] cluster fusion on ISCA1–ISCA2 by
699 electron flow from ferredoxin FDX2. Proc Natl Acad Sci U S A 2020;117:20555–65.
700 43 Schilke B, Voisine C, Beinert H, Craig E. Evidence for a conserved system for iron
701 metabolism in the mitochondria of *Saccharomyces cerevisiae*. Proc Natl Acad Sci U S
702 A 1999;96:10206–11.
703 44 Jensen LT, Culotta VC. Role of Saccharomyces cerevisiae ISA1 and ISA2 in Iron
704 Homeostasis . Molecular and Cellular Biology 2000;20:3918–27.
705 45 Rodríguez-Manzaneque MT, Tamarit J, Bellí G, Ros J, Herrero E. Grx5 is a
706 mitochondrial glutaredoxin required for the activity of iron/sulfur enzymes. Molecular
707 Biology of the Cell 2002;13:1109–21.
708 46 Yang J, Wagner SA, Beli P. Illuminating spatial and temporal organization of protein
709 interaction networks by mass spectrometry-based proteomics. Frontiers in Genetics
710 2015;6:344.
711 47 Roland M, Przybyla-Toscano J, Vignols F, Berger N, Azam T, Christ L, et al. The
712 plastidial *Arabidopsis thaliana* NFU1 protein binds and delivers [4Fe-4S] clusters to
713 specific client proteins. Journal of Biological Chemistry 2020;295:1727–42.
714 48 Leitsch D, Müller J, Müller N. Evaluation of *Giardia lamblia* thioredoxin reductase as
715 drug activating enzyme and as drug target. International Journal for Parasitology: Drugs
716 and Drug Resistance 2016;6:148–53.

717 49 Rout S, Zumthor JP, Schraner EM, Faso C, Hehl AB. An interactome-centered protein
718 discovery approach reveals novel components involved in mitosome function and
719 homeostasis in *Giardia lamblia*. PLOS Pathogens 2016;12:e1006036.
720 50 Dagley MJ, Dolezal P, Likic VA, Smid O, Purcell AW, Buchanan SK, et al. The protein
721 import channel in the outer mitosomal membrane of *Giardia intestinalis*. Mol Biol Evol
722 2009;26:1941–7.
723 51 Pain D, Dancis A. Roles of Fe–S proteins: from cofactor synthesis to iron homeostasis
724 to protein synthesis. Current Opinion in Genetics & Development 2016;38:45–51.
725 52 Van Vranken JG, Na U, Winge DR, Rutter J. Protein-mediated assembly of succinate
726 dehydrogenase and its cofactors. Critical Reviews in Biochemistry and Molecular
727 Biology 2015;50:168–80.
728 53 Beinert H, Kennedy MC, Stout CD. Aconitase as iron−sulfur protein, enzyme, and iron-
729 regulatory protein. Chemical Reviews 1996;96:2335–73.
730 54 Przybyla-Toscano J, Christ L, Keech O, Rouhier N. Iron–sulfur proteins in plant
731 mitochondria: roles and maturation. Journal of Experimental Botany 2021;72:2014–44.
732 55 Jain A, Singh A, Maio N, Rouault TA. Assembly of the [4Fe–4S] cluster of NFU1
733 requires the coordinated donation of two [2Fe–2S] clusters from the scaffold proteins,
734 ISCU2 and ISCA1. Human Molecular Genetics 2020;29:3165–82.
735 56 Bremer H, Dennis PP. Respiration. In: Neidhardt FC, editor. Escherichia coli and
736 Salmonella: cellular and molecular biology. 2nd ed., ASM Press; 1996, p. 217–61.
737 57 Valasatava Y, Rosato A, Banci L, Andreini C. MetalPredator: A web server to predict
738 iron-sulfur cluster binding proteomes. Bioinformatics 2016;32:2850–2.
739 58 Pyrih J, Pyrihová E, Kolísko M, Stojanovová D, Basu S, Harant K, et al. Minimal
740 cytosolic iron-sulfur cluster assembly machinery of *Giardia intestinalis* is partially
741 associated with mitosomes. Molecular Microbiology 2016;102:701–14.

59 Talib EA, Outten CE. Iron-sulfur cluster biogenesis, trafficking, and signaling: Roles for CGFS glutaredoxins and BolA proteins. Biochim Biophys Acta Mol Cell Res 2021;1868.

60 Horáčková V, Voleman L, Hagen KD, Petrů M, Vinopalová M, Weisz F, et al. CRISPR/Cas9-mediated gene disruption in the tetraploid protist *Giardia intestinalis*. Open Biology 2022:2021.04.21.440745.

61 Jarroll EL, van Keulen H, Paget TA, Lindmark DG. Giardia Metabolism. In: Luján HD, Svärd S, editors. Giardia: A Model Organism, Vienna: Springer Vienna; 2011, p. 127–37.

62 Goldberg A v., Molik S, Tsaousis AD, Neumann K, Kuhnke G, Delbac F, et al. Localization and functionality of microsporidian iron–sulphur cluster assembly proteins. Nature 2008;452:624–8.

63 Lill R. From the discovery to molecular understanding of cellular iron-sulfur protein biogenesis. Biological Chemistry 2020;401:855–76.

64 Dolezal P, Dancis A, Lesuisse E, Sutak R, Hrdý I, Embley TM, et al. Frataxin, a conserved mitochondrial protein, in the hydrogenosome of *Trichomonas vaginalis*. Eukaryot Cell 2007;6:1431–8.

65 Sutak R, Dolezal P, Fiumera HL, Hrdy I, Dancis A, Delgadillo-Correa M, et al. Mitochondrial-type assembly of FeS centers in the hydrogenosomes of the amitochondriate eukaryote *Trichomonas vaginalis*. Proc Natl Acad Sci U S A 2004;101:10368–73.

66 Tsaousis AD. On the origin of iron/sulfur cluster biosynthesis in eukaryotes. Frontiers in Microbiology 2019;10.

67 Rouault TA. Biogenesis of iron-sulfur clusters in mammalian cells: new insights and relevance to human disease. Disease Models & Mechanisms 2012;5:155–64.

767 68 Pain D, Dancis A. Roles of Fe–S proteins: from cofactor synthesis to iron homeostasis
768 to protein synthesis. Current Opinion in Genetics & Development 2016;38:45–51.
769 69 Frey AG, Palenchar DJ, Wildemann JD, Philpott CC. A glutaredoxin·BolA complex
770 serves as an iron-sulfur cluster chaperone for the cytosolic cluster assembly machinery.
771 The Journal of Biological Chemistry 2016;291:22344.
772 70 Sen S, Rao B, Wachnowsky C, Cowan JA. Cluster exchange reactivity of [2Fe-2S]
773 cluster-bridged complexes of BOLA3 with monothiol glutaredoxins. Metallomics
774 2018;10:1282–90.
775 71 Voleman L, Najdrová V, Ástvaldsson Á, Tůmová P, Einarsson E, Švindrych Z, et al.
776 *Giardia intestinalis* mitosomes undergo synchronized fission but not fusion and are
777 constitutively associated with the endoplasmic reticulum. BMC Biology 2017;15:1–27.
778 72 Kispal G, Csere P, Prohl C, Lill R. The mitochondrial proteins Atm1p and Nfs1p are
779 essential for biogenesis of cytosolic Fe/S proteins. The EMBO Journal 1999;18:3981–9.
780 73 Jumper J, Evans R, Pritzel A, Green T, Figurnov M, Ronneberger O, et al. Highly
781 accurate protein structure prediction with AlphaFold. Nature 2021 596:7873
782 2021;596:583–9.
783 74 Valasatava Y, Rosato A, Banci L, Andreini C. MetalPredator: a web server to predict
784 iron–sulfur cluster binding proteomes. Bioinformatics 2016;32:2850–2.
785 75 Füssy Z, Vinopalová M, Treitli SC, Pánek T, Smejkalová P, Čepička I, et al.
786 Retortamonads from vertebrate hosts share features of anaerobic metabolism and pre-
787 adaptations to parasitism with diplomonads. Parasitology International 2021;82:102308.
788 76 Yazaki E, Kume K, Shiratori T, Eglit Y, Tanifuji G, Harada R, et al. Barthelonids
789 represent a deep-branching metamonad clade with mitochondrion-related organelles
790 predicted to generate no ATP. Proc Biol Sci 2020;287.

77 Fu L, Niu B, Zhu Z, Wu S, Li W. CD-HIT: Accelerated for clustering the next-generation sequencing data. Bioinformatics 2012;28:3150–2.

78 Katoh K, Standley DM. MAFFT multiple sequence alignment software version 7: improvements in performance and usability. Mol Biol Evol 2013;30:772–80.

79 Capella-Gutiérrez S, Silla-Martínez JM, Gabaldón T. trimAl: A tool for automated alignment trimming in large-scale phylogenetic analyses. Bioinformatics 2009;25:1972–3.

80 Minh BQ, Schmidt HA, Chernomor O, Schrempf D, Woodhams MD, von Haeseler A, et al. IQ-TREE 2: New Models and Efficient Methods for Phylogenetic Inference in the Genomic Era. Molecular Biology and Evolution 2020;37:1530–4.

81 Dolezal P, Smíd O, Rada P, Zubácová Z, Bursać D, Suták R, et al. *Giardia* mitosomes and trichomonad hydrogenosomes share a common mode of protein targeting. Proc Natl Acad Sci U S A 2005;102:10924–9.

82 Najdrová V, Stairs CW, Vinopalová M, Voleman L, Doležal P. The evolution of the Puf superfamily of proteins across the tree of eukaryotes. BMC Biology 2020;18:1–18.

83 Keister DB. Axenic culture of *Giardia lamblia* in TYI-S-33 medium supplemented with bile. Trans R Soc Trop Med Hyg 1983;77:487–8.

84 Dagley MJ, Dolezal P, Likić VA, Smid O, Purcell AW, Buchanan SK, et al. The protein import channel in the outer mitosomal membrane of Giardia intestinalis. Molecular Biology and Evolution 2009;26:1941–7.

85 Martincová E, Voleman L, Najdrová V, De Napoli M, Eshar S, Gualdron M, et al. Live imaging of mitosomes and hydrogenosomes by HaloTag technology. PLoS One 2012;7:e36314.

86 Schneider CA, Rasband WS, Eliceiri KW. NIH Image to ImageJ: 25 years of image analysis. Nat Methods 2012;9:671–5.

87 Cox J, Mann M. MaxQuant enables high peptide identification rates, individualized p.p.b.-range mass accuracies and proteome-wide protein quantification. Nature Biotechnology 2008;26:1367–72.

88 Cox J, Neuhauser N, Michalski A, Scheltema RA, Olsen J v., Mann M. Andromeda: A peptide search engine integrated into the MaxQuant environment. Journal of Proteome Research 2011;10:1794–805.

89 Tyanova S, Temu T, Sinitcyn P, Carlson A, Hein MY, Geiger T, et al. The Perseus computational platform for comprehensive analysis of (prote)omics data. Nature Methods 2016;13:731–40.

90 Goedhart J, Luijsterburg MS. VolcaNoseR is a web app for creating, exploring, labeling and sharing volcano plots. Scientific Reports 2020 10:1 2020;10:1–5.

91 Metsalu T, Vilo J. ClustVis: a web tool for visualizing clustering of multivariate data using Principal Component Analysis and heatmap. Nucleic Acids Research 2015;43:W566–70.

92 Pyrihová E, Motyčková A, Voleman L, Wandyszewska N, Fišer R, Seydlová G, et al. A single Tim translocase in the mitosomes of *Giardia intestinalis* illustrates convergence of protein import machines in anaerobic eukaryotes. Genome Biology and Evolution 2018;10:2813–22.

841

842

843

844

845

846

847

848

849

850

851

852 **FIGURES AND FIGURE LEGENDS**

853

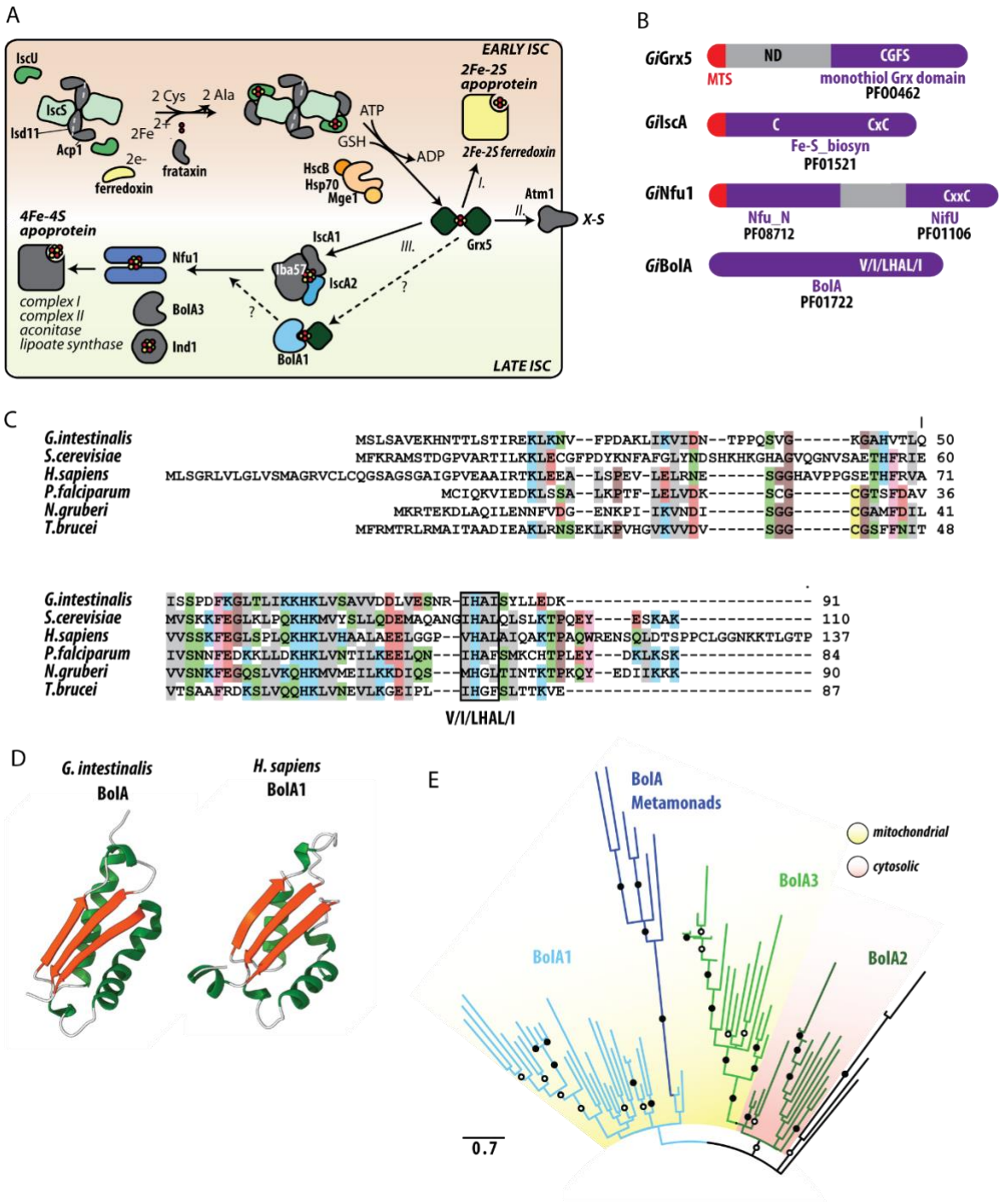

Figure 1. Components of late ISC pathway in *G. intestinalis*.

(A) Schematic representation of mitosomal ISC pathway. The mitochondrial components that are missing in *Giardia* mitosomes are shown in grey. Early and late ISC pathway is distinguished by the background colour, [2Fe-2S] cluster on Grx5 dimer can be (*I.*) transferred to the target mitochondrial apoproteins (*II.*) exported to the cytosol or (*III.*) enters the late ISC machinery.

(B) Domain structure of *Gi*Grx5, *Gi*IscA, *Gi*Nfu1, and *Gi*BolA. The respective sequence motifs and Pfam accession numbers are shown. (C) Protein sequence alignment of the identified *Gi*BolA with the homologues from, *Saccharomyces cerevisiae* (Q3E793), *Homo sapiens* (Q9Y3E2), *Plasmodium falciparum* (Q8I3V0), *Naegleria gruberi* (D2V472) and *Trypanosoma brucei* (Q57YM0). BolA signature V/I/LHAL/I motif is highlighted. (D) Structure of *Gi*BolA as predicted by AlphaFold2 (73), predicted structure of human BolA1 (*Hs*BolA1) (27) is shown for comparison. (E) Maximum likelihood phylogenetic tree of 70 eukaryotic BolA1 paralogues shows that *Gi*BolA and metamonad BolA homologues emerge from within a clade of mitochondrial BolA1 proteins. Summary of bipartition support values (1000 ultrafast bootstraps) greater than 80 or 95 are shown in open and closed circles, respectively.

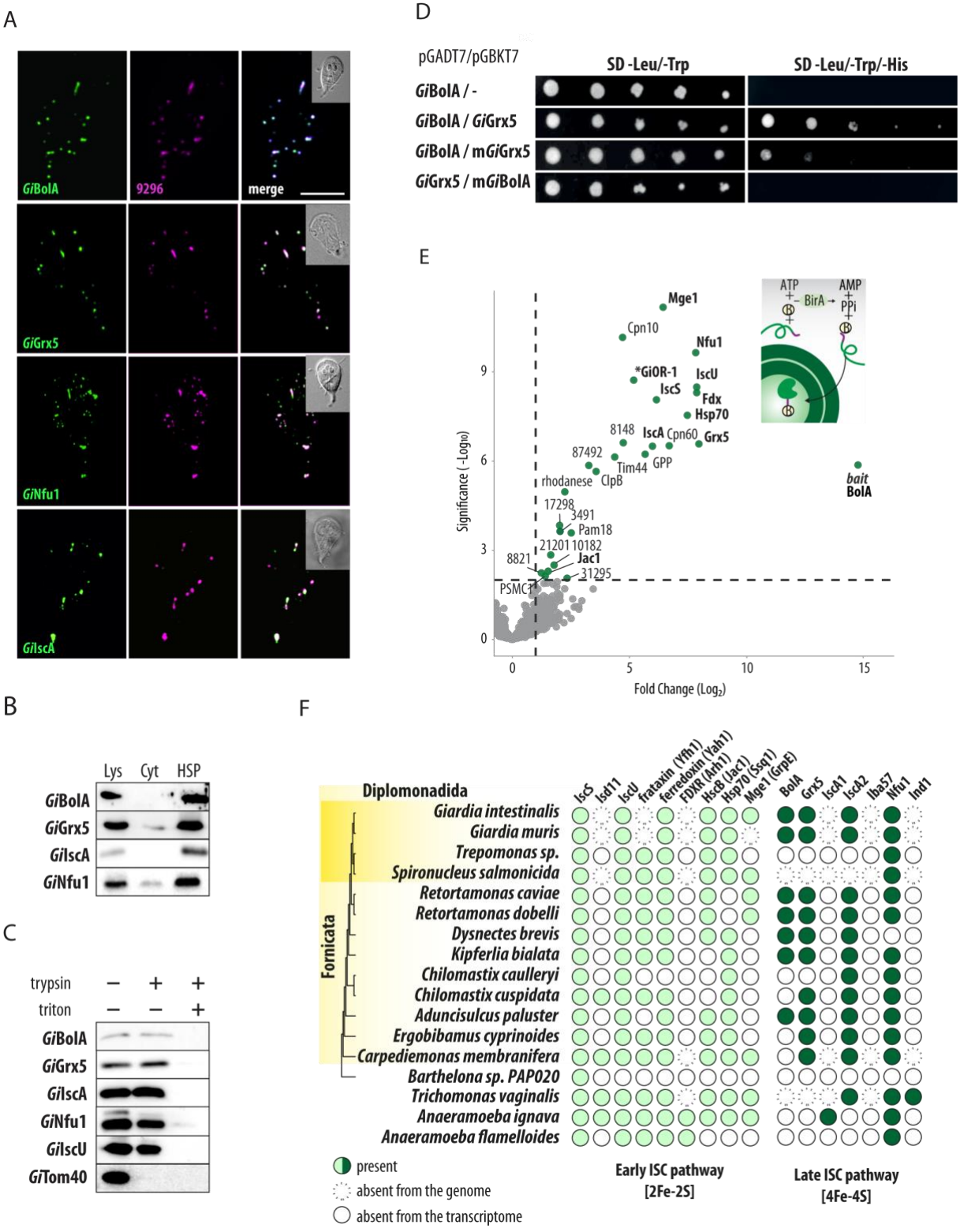

Figure 2. *Gi*BolA is a mitosomal protein that specifically interacts with *Gi*Grx5 and other ISC components. (A) BAP-tagged *Gi*BolA, *Gi*Grx5, *Gi*Nfu1 and *Gi*IscA were expressed in *G. intestinalis* and the proteins were detected by anti-BAP antibody (green). The

co-colocalization with mitosomal marker GL50803_9296 (magenta) is shown. The DIC image of the cell is shown in the inlet, the scale bar represents 5 μm. (B) Detection of BAP-tagged *Gi*BolA, *Gi*Grx5, *Gi*Nfu1 and *Gi*IscA in cellular fractions, lys – cell lysate, cyt - cytosol, HSP – high speed pellet fraction. (C) Protease protection assay of late ISC components and the markers of the outer mitosomal membrane (*Gi*Tom40) and the mitosomal matrix (*Gi*IscU). High-speed pellets isolated from *G. intestinalis* expressing BAP-tagged *Gi*BolA, *Gi*Grx5 *Gi*IscA and *Gi*Nfu1 were incubated with 20 μg/ml trypsin and 0.1% Triton X-100. The samples were immunolabeled with antibodies against the BAP tag, *Gi*Tom40 and *Gi*IscU. (D) Serial dilutions of Y2H assay testing the protein interactions between *Gi*BolA and *Gi*Grx5. The introduction of specific mutations of conserved residues (H90A *Gi*BolA and C128A *Gi*Grx5) abolished the interaction, double and triple dropout medium was used to test the presence of the plasmids and the interaction of the encoded proteins, respectively. (E) Affinity purification of the *in vivo* biotinylated *Gi*BolA with the DSP-crosslinked interacting partners. (top right) Scheme of the *in vivo* biotinylation of the C-terminal BAP-tag of *Gi*BolA by cytosolic BirA. (left) Volcano plot of the statistically significant hits obtained from the protein purification on streptavidin coupled Dynabeads. Components involved in ISC pathway are shown in bold letters. (F) The presence/absence of the ISC components in Metamonada supergroup.

914

915

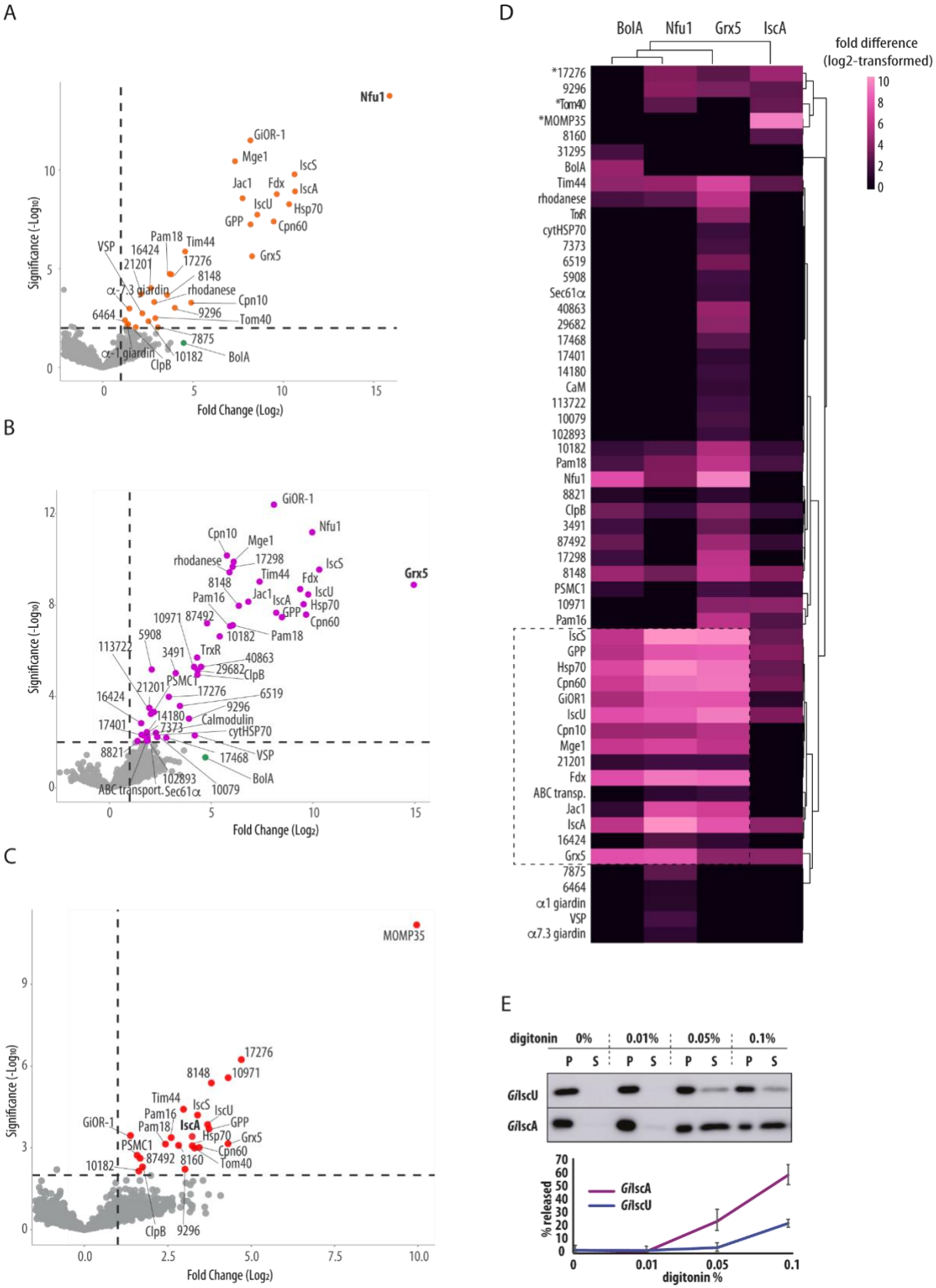

916

917 **Figure 3. Proteomic analysis of late ISC pathway.** BAP-tagged *Gi*Grx5, *Gi*Nfu1 and

918 *Gi*IscA

were *in vivo* biotinylated by cytosolic BirA and purified on streptavidin-coupled Dynabeads upon crosslinking by DSP. (A-C) Volcano plots depict the significantly enriched proteins that co-purified with (A) *Gi*Nfu1, (B) *Gi*Grx5 and (C) *Gi*IscA. (D) Heatmap of combined significantly enriched proteins for all four late ISC components, (E) Digitonin solubilization of the mitosomes shows differential release of IscA over IscU, P -pellet fraction (retained protein), S – supernatant (released protein). Exemplary western blot of four independent experiments is shown, the error bars show standard deviation.

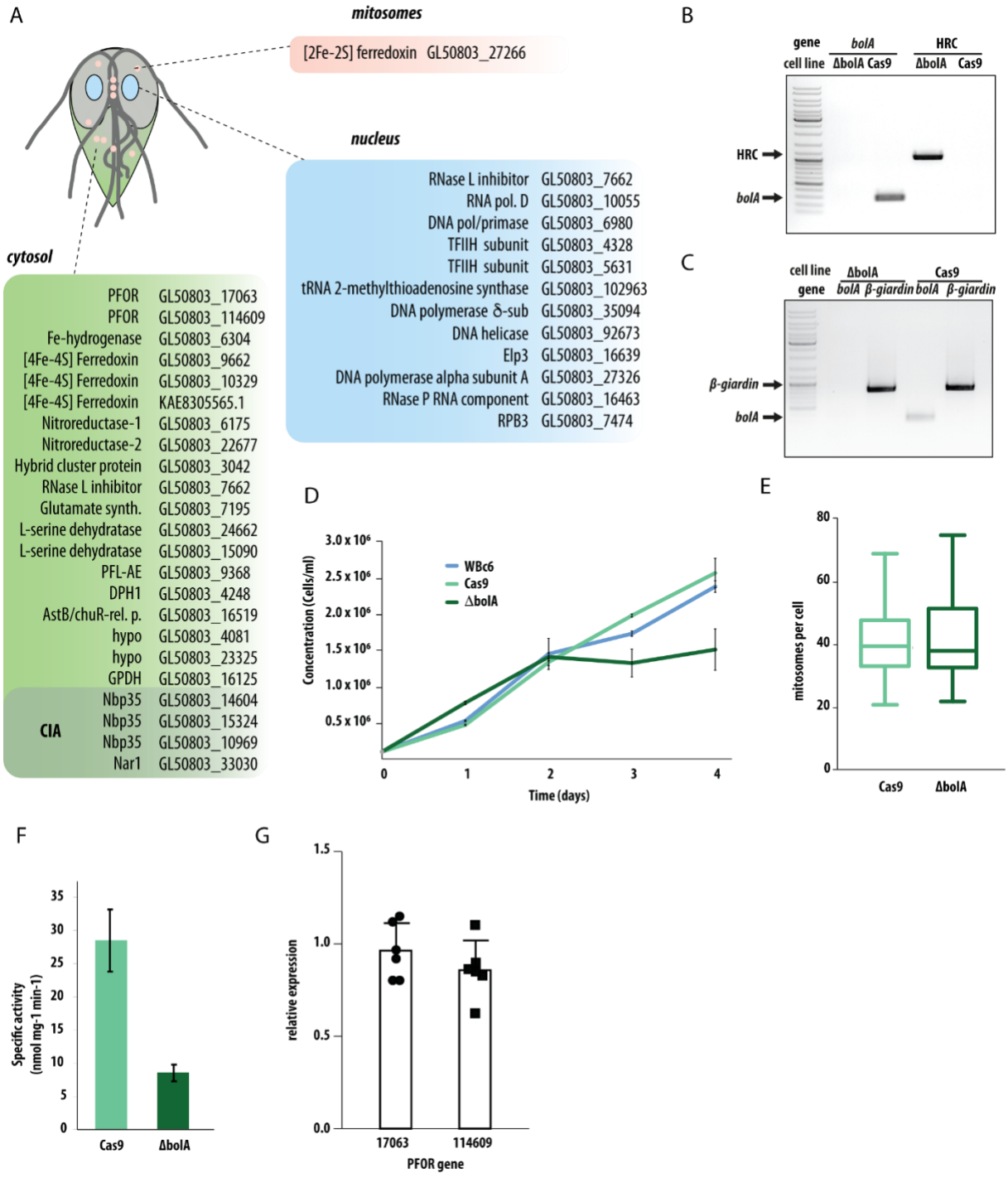

943

944 **Figure 4. Mitosomal *Gi*BolA is involved in the formation of cytosolic Fe-S proteins.** (A)
945 The list of predicted 40 Fe-S proteins in *G. intestinalis* includes only one mitosomal protein,
946 [2Fe-2S] ferredoxin, that itself participates in the ISC pathway. All putative clients that
947 require [4Fe-4S] clusters are localized in the cytosol or in the nucleus (Supplementary Table
948 3). (B) The ΔbolA cell line was tested for the presence of *bolA* gene and the integration of
949 homologous recombination cassette (HRC) by PCR on gDNA, (C) the expression of *bolA*

gene in ΔbolA cell line was tested by PCR on the cDNA, *β-giardin* was used as a control gene. (D) The slowed growth phenotype of ΔbolA cell line in comparison to parental Cas9-expressing cell line and wildtype WBc6 strain, error bars represent standard deviation. (E) The number of mitosomes per cells in Cas9-expressing (n=64) and ΔbolA cells (n=107), the error bars of the box plot depict min to max values.

(F) Decreased activity of cytosolic PFOR in ΔbolA cell line when compared to the parental Cas9-expressing cell line, the error bars depict standard deviation.

(F) Real-time PCR results show relative expression of two PFOR-encoding genes, GL50803_17063 and GL50803_114609, in ΔbolA cell line. Expression levels are depicted relative to the control cell line. Calculated results from six independent RNA isolations are shown for each gene. The expression of both genes was normalized to NADH oxidase-encoding gene, GL50803_33796. Cas9-expressing cell line was used as a control, the error bars depict standard deviation.

SUPPLEMENTARY DATA

Supplementary Figure 1

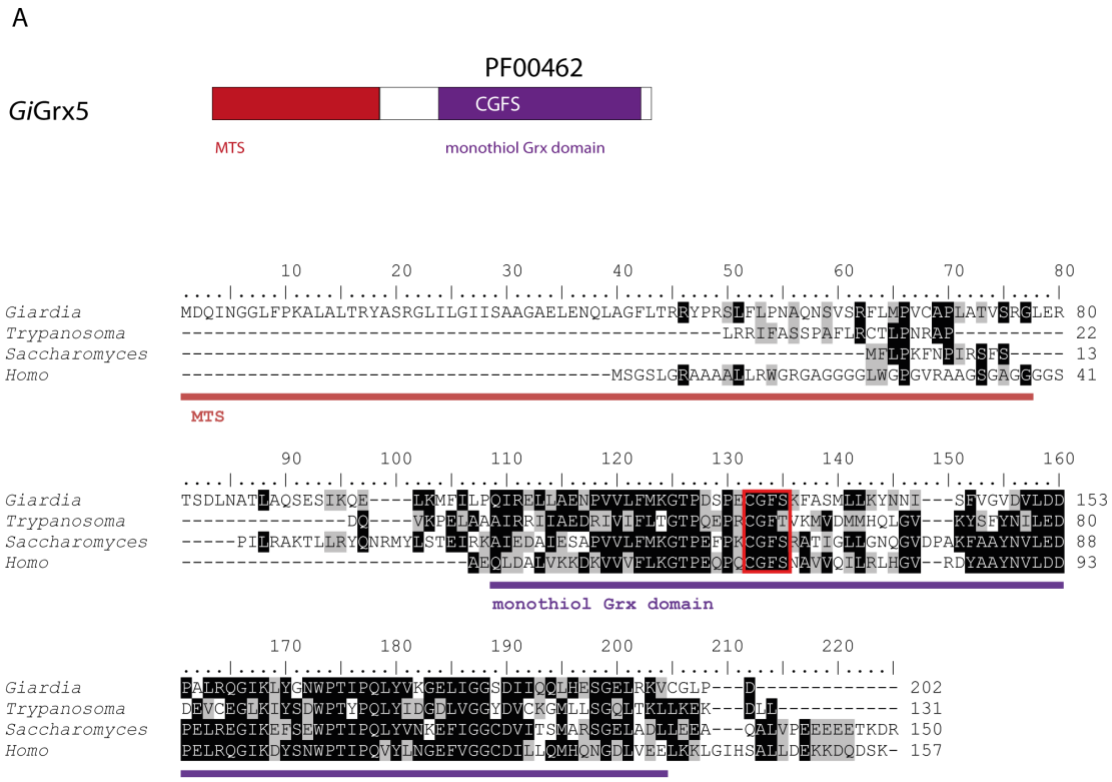

B

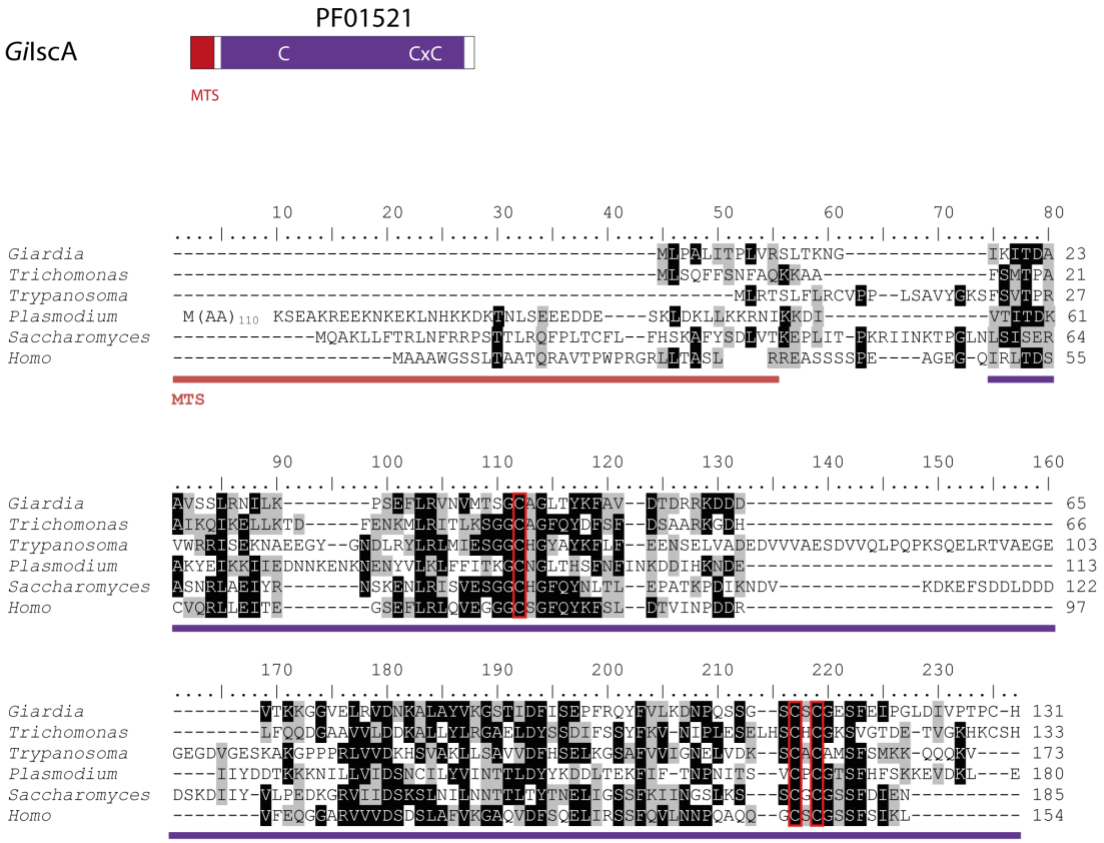

986

987

988

989

C

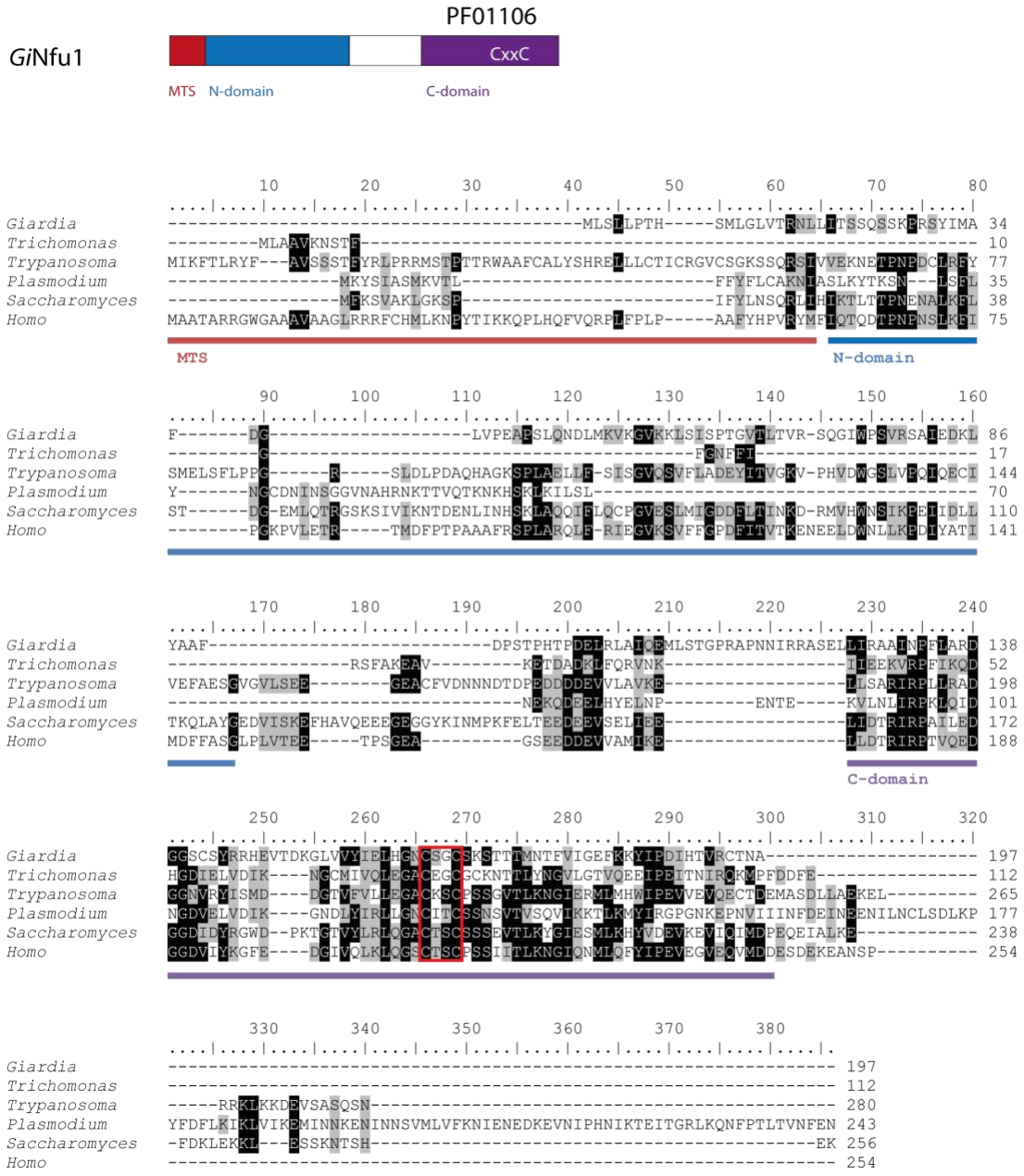

990

991

992

993 **Supplementary Figure 1. Protein sequence alignments of late ISC components of *Giardia***

994 ***intestinalis.*** (A) Grx5, the diagram shows the domain structure of *Gi*Grx5, mitochondrial

995 targeting sequence (MTS) is shown in red, monothiol glutaredoxin domain (PF00462) in

996 purple, the CGFS motif is also highlighted. (B) *Gi*IscA shares the Fe-S_biosyn domain

997 (PF01521) with the conserved cysteine residues involved in cluster binding. (C) *Gi*Nfu1

contains conserved N- and C- domains, the latter of is recognized as NifU domain (PF01106) and carries conserved cysteine motif.

Supplementary Figure 2

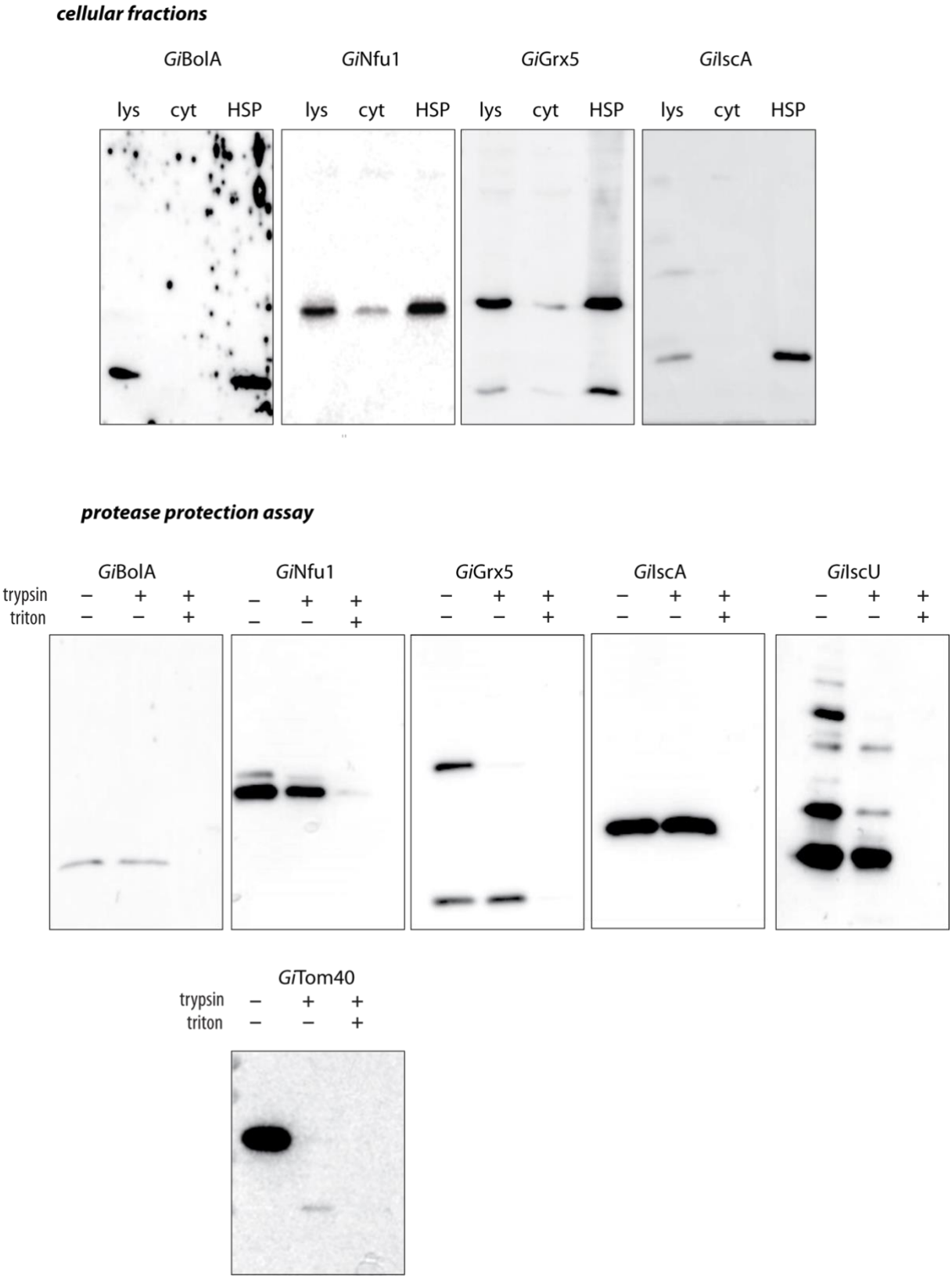

Supplementary Figure 2. Full blots of cellular fractions and protease protection assay experiments.

Supplementary Figure 3

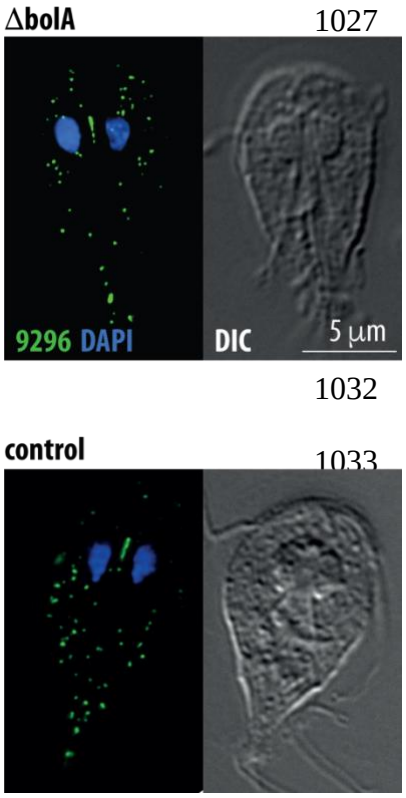

Supplementary Figure 3. Mitosomal morphology and number is not affected by the removal of *bolA* gene. The exemplary image of mitosomes visualized by immunofluorescence microscopy in the ΔbolA and control (Cas9) cell lines. Mitosomes were detected by rabbit polyclonal antibody raised against GL50803_9296, the nuclei were stained with DAPI.

Supplementary Table 1. Proteomic analysis of *Gi*BolA, *Gi*Grx5, *Gi*Nfu1 and *Gi*IscA pulldowns. For all proteins, statistical analysis based upon the biological and technical triplicates are shown.

Supplementary Table 2. ISC components of Metamonada

Supplementary Table 3. Fe-S proteins of *G. intestinalis.*

Supplementary Table 4. Proteomic analysis of ΔbolA cell line.

Supplementary Table 5. Primers used in the study.